



Article

Topology Optimization of Anisotropic Materials with Smooth Fiber Orientation

Shaofei Jiang ¹, Chaofan Shang ¹, Jiquan Li ^{1,2}, Bing Yi ³ and Xiang Peng ^{1,2,*}¹ College of Mechanical Engineering, Zhejiang University of Technology, Hangzhou 310023, China² Taizhou Key Laboratory of Advanced Manufacturing Technology, Taizhou Institute, Zhejiang University of Technology, Taizhou 318014, China³ School of Traffic and Transportation Engineering, Central South University, Changsha 410083, China

* Correspondence: pengxiang@zjut.edu.cn

Abstract: In the concurrent optimization of topology and fiber orientation, the design of smooth fiber helps to maintain the stability of numerical calculation and the compatibility of the manufacturing process. However, the improvement of fiber continuity is often accompanied by a significant decrease in the overall structural stiffness. Aiming at this problem, this paper proposes a topology optimization method for anisotropic materials with smooth fiber orientation. This method improves the smoothness of fiber orientation and reduces stiffness loss by introducing a fiber angle constraint strategy and adaptive filtering technology. The fiber angle constraint strategy integrates the created angle constraint function into the Method of Moving Asymptotes (MMA) to complete the strong constraint of the angle. This strategy quantifies the continuity of the fiber and effectively improves the continuity of the fiber. At the same time, the application of adaptive filtering technology can adjust a reasonable fiber angle distribution on the basis of smoothing fibers, thereby enhancing the stiffness of the overall structure. In addition, this paper shows the complete optimization process and MATLAB code implementation and verifies the effectiveness of the method through a series of numerical examples, that is, on the basis of improving fiber continuity, the stiffness of the whole structure is guaranteed, and then the effective balance between the two is realized.

Keywords: topology optimization; concurrent optimization; fiber angle constraint; adaptive filtering; MATLAB implementation



Citation: Jiang, S.; Shang, C.; Li, J.; Yi, B.; Peng, X. Topology Optimization of Anisotropic Materials with Smooth Fiber Orientation. *Appl. Sci.* **2024**, *14*, 5947. <https://doi.org/10.3390/app14135947>

Academic Editor: Ana Martins Amaro

Received: 4 April 2024

Revised: 25 June 2024

Accepted: 2 July 2024

Published: 8 July 2024



Copyright: © 2024 by the authors. Licensee MDPI, Basel, Switzerland. This article is an open access article distributed under the terms and conditions of the Creative Commons Attribution (CC BY) license (<https://creativecommons.org/licenses/by/4.0/>).

1. Introduction

Topology optimization [1] has attracted much attention in structural design, especially in the industrial field to deal with lightweight requirements. Traditional methods are not enough to meet the requirements, so fiber-reinforced composites [2] have become the focus of optimization, which means that in addition to topology optimization of the overall structure, the best orientation of the material must also be considered.

The fiber orientation is generally defined by the fiber angle of the discrete element. The fiber angle optimization is divided into discrete material optimization (DMO) [3–6] and continuous fiber angle optimization (CFAO) [7–11]. Unlike DMO, which is not easy to converge and has limited candidate angles, CFAO is more widely used. It is no longer limited to a set of candidate angles in a specified direction but takes the continuous rotation angle of the anisotropic substrate as a design variable. Therefore, CFAO is favored by many scholars in the concurrent optimization of topology and the fiber angle.

Many scholars have proposed different methods in the study of CFAO topology optimization, aiming at improving fiber continuity. Based on the improved SIMP method [12], Chen [13] used the volume control and stress control algorithm to optimize the topology in two stages to obtain the optimal structural topology of isotropic materials. After establishing the average load transfer trajectory in the optimal topology, the fiber reinforcement placement path is defined for the main continuous fiber filling area. The two-stage

topology design makes the structural mechanical performance better, and the streamline method makes the fiber laying smoother. Duvaut et al. [14] conducted in-depth research on the optimal fiber orientation and fiber volume ratio under the constraint of the fiber cost function and proposed a classical compliance minimization solution, but the problem expression they used is not a traditional topology optimization equation. In the framework of cellular automata, Setoodeh [15] obtained a smooth distribution of fiber angles by averaging adjacent fiber angles. This method is similar to using a mean filter to adjust the fiber angle, which often leads to excessive smoothing of the fiber angle. Similarly, Panesar and Weaver [16] proposed a cooperative design strategy by imposing angle constraints between adjacent elements to ensure that bidirectional constraints are satisfied. This method effectively coordinates the design of fiber orientation so that it can meet the specific mechanical performance requirements while maintaining structural integrity. Desai [17] described a three-phase method to optimize the orientation of continuous fibers in isotropic materials. This method allows the design of composite materials with variable stiffness, where the fiber volume fraction and the orientation of each node are considered stiffness design variables [18,19]. Peeters et al. [20] skillfully applied the curvature constraint of the fiber angle in the optimization process and carefully smoothed the optimization results to enhance manufacturability.

In the topology optimization of anisotropic materials, filtering or projection techniques are widely used, which play an important role in the whole optimization process. The application of these technologies can not only effectively avoid numerical instability but also improve the manufacturability of the optimization results. Therefore, the appropriate filtering method injects deep robustness and feasibility into the concurrent optimization method of structural topology and the smoothing fiber angle.

It is of great significance to use the filtering technology to control the fiber orientation in the CFAO method, which can avoid the stress concentration caused by the excessive curvature of the fiber and solve the manufacturing constraints related to the curvature of the fiber in the subsequent printing. In the topology optimization of anisotropic materials, Jantos [21] combined a filtering technique applied to the material stiffness tensor, which is not limited to the actual parameterization of the design variables and can control the smoothness of the fiber path. Huang [22] combined the characteristics of two design variables, regarded the density material variable in the element as the weight factor of fiber orientation, and completed the adjustment of fiber orientation to create a continuous fiber trajectory direction. Similarly, Schmidt [23] greatly reduced the curvature of the fiber path by keeping the filter radius of the fiber angle consistent with the mesh resolution and applied it to the optimization of the three-dimensional structure. Papapetrou et al. [24] completed the material layout and fiber angle optimization of orthotropic materials through the density-based method (SOMP) and demonstrated the EQS method, streamline method, and offset method fiber filling schemes based on density-based topology optimization. The manufacturability is high, but this post-processing method often leads to lower structural stiffness. Boddeti [25] discussed the optimal design methods of variable stiffness laminated continuous fiber-reinforced composites and transformed these designs into actual manufacturing processes. More prospectively, Chandrasekhar [26] introduces a new method called FRC-TOuNN, which uses neural networks to perform topology optimization of continuous fiber-reinforced composites. This method combines machine learning techniques and topology optimization algorithms to improve the efficiency and accuracy of the design process, especially when dealing with complex fiber paths and load conditions.

However, for the concurrent optimization of topology and the fiber angle, although the above fiber angle optimization strategy and filtering technology significantly improve fiber continuity, there are two obvious defects: it is impossible to quantify the degree of fiber continuity and achieve accurate optimization goals and in the pursuit of fiber smoothness, too much of the stiffness of the overall structure is sacrificed.

In view of the above problems, this paper proposes a topology optimization method for anisotropic materials with smooth fiber orientation, which introduces the fiber angle

constraint strategy and adaptive filtering technology. The fiber angle constraint strategy can quantify the degree of fiber continuity and effectively improve fiber continuity. At the same time, the application of adaptive filtering technology can adjust a reasonable fiber angle distribution on the basis of smoothing fibers, thereby enhancing the stiffness of the overall structure. Therefore, the combination of the fiber angle constraint strategy and adaptive filtering technology can accurately improve fiber continuity while ensuring overall structural stiffness. Specifically, the proposed method aims to meet the following criteria:

1. The fiber angle constraint function is created and integrated into the Method of Moving Asymptotes (MMA) [25] to accurately improve fiber continuity;
2. The Gaussian function is used to filter the fiber angle adaptively, and the strength of the filter is controlled by dynamically adjusting the standard deviation of the Gaussian function so as to realize the reasonable distribution of the fiber angle and further improve the structural stiffness;
3. The whole optimization process is realized by MATLAB R2021a, and the code structure is easy to understand and implement (see Appendix A).

The organizational structure of this paper is as follows. Section 2 first introduces the concurrent optimization framework based on density. On this basis, it expounds the constraint strategy and adaptive filtering technology of the fiber angle and shows the complete optimization process and MATLAB code implementation. In Section 3, a large number of numerical examples are analyzed. Through a series of numerical examples, the structural stiffness, fiber continuity, and numerical stability are analyzed in depth, and the effectiveness and practicability of the proposed method are verified.

2. Model Derivation

This section introduces the model derivation of the topology optimization method for anisotropic materials with smooth fiber orientation. Firstly, taking the single-layer fiber-reinforced composite as the research object, the mathematical model is established with the unit density and the unit fiber angle in the design domain as the design variables. Then, the fiber angle constraint function is created, and the smoothing mechanism of the constraint function to the fiber angle is introduced. The fiber angle is updated by the MMA algorithm. In addition, for the problem of structural stiffness reduction caused by the constraint function, the fiber angle is adaptively filtered to further standardize the reasonable distribution of the fiber angle, and the stiffness of the overall structure is improved while smoothing the fiber.

2.1. Density-Based Concurrent Optimization Framework

The topology optimization framework proposed in this paper is an extension of the Solid Isotropic Material with Penalization (SIMP) method to orthotropic materials and combined with the CFAO method for concurrent optimization. Four-point element discretization is performed for a given design domain. For each element, element density (material distribution) and the fiber angle (element fiber orientation) are considered design variables. With compliance as the objective function, the volume fraction and fiber continuity rate are forced as constraints, and the mathematical optimization model is as follows:

$$\begin{aligned}
 \min C(\mathbf{x}, \boldsymbol{\theta}) &= \mathbf{U}^T \cdot \mathbf{K} \cdot \mathbf{U} = \sum_{e=1}^N x_e^p \mathbf{u}_e^T \cdot \mathbf{k}_\theta^e \cdot \mathbf{u}_e \\
 \text{s.t. } &\mathbf{K} \cdot \mathbf{U} = \mathbf{F}, \\
 &\frac{V(\mathbf{x})}{V_0} \leq \text{volfrac}, \\
 &f(\boldsymbol{\theta}) > 0, \\
 &x_e \in [0, 1], \\
 &\theta_e \in \left[-\frac{\pi}{2}, \frac{\pi}{2}\right]
 \end{aligned} \tag{1}$$

where C represents the compliance, x is the density, θ is the fiber angle, C is the function of x_e and θ_e , p is the penalty factor, \mathbf{U} and \mathbf{K} are the global displacement and global stiffness matrix, respectively, and x_e , \mathbf{k}_θ^e , and \mathbf{u}_e represent the element density, element stiffness matrix, and node displacement matrix of element e . \mathbf{F} is the force vector, $V(x)$ and V_0 are the material volume and the design domain volume, respectively, `volfrac` is the predefined volume fraction, and $f(\theta)$ is the fiber angle constraint function.

In anisotropic materials, we calculate the compliance coefficient matrix in the natural coordinate system by introducing the transformation matrix \mathbf{T} as follows:

$$\mathbf{D} = \mathbf{T}^{-1} \mathbf{C} (\mathbf{T}^{-1})^T \tag{2}$$

where \mathbf{T} is the coordinate transformation matrix and \mathbf{C} is the compliance coefficient in the main coordinate system. \mathbf{C} and \mathbf{T} are calculated as follows:

$$\mathbf{C} = \begin{bmatrix} \frac{E_1}{1-\nu_{12}\nu_{21}} & \frac{\nu_{12}E_2}{1-\nu_{12}\nu_{21}} & 0 \\ \frac{\nu_{21}E_1}{1-\nu_{12}\nu_{21}} & \frac{E_2}{1-\nu_{12}\nu_{21}} & 0 \\ 0 & 0 & G_{12} \end{bmatrix} \tag{3}$$

$$\mathbf{T} = \begin{bmatrix} \cos^2 \theta & \sin^2 \theta & \sin 2\theta \\ \sin^2 \theta & \cos^2 \theta & -\sin 2\theta \\ -\cos \theta \sin \theta & \cos \theta \sin \theta & \cos^2 \theta - \sin^2 \theta \end{bmatrix} \tag{4}$$

Among them, fiber-reinforced composites are regarded as orthotropic materials, and there is $\frac{\nu_{12}}{E_2} = \frac{\nu_{21}}{E_1}$. Therefore, in the plane stress problem, orthotropic materials have four independent elastic constants, E_1 , E_2 , ν_{21} , and G_{12} , which represent the longitudinal elastic modulus, transverse elastic modulus, longitudinal Poisson’s ratio, and shear modulus, respectively, and θ is the fiber angle.

Then, the element stiffness matrix of all elements is calculated as follows:

$$\mathbf{k}_\theta = \iint \mathbf{B}^T \mathbf{D} \mathbf{B} dx dy \tag{5}$$

where \mathbf{k}_θ is the element stiffness matrix after counterclockwise rotation t , \mathbf{B} is the strain–stress matrix, and \mathbf{D} is the flexibility coefficient matrix in the natural coordinate system.

Then, all element stiffness matrices are assembled into a global stiffness matrix \mathbf{K} . According to the equilibrium equation $\mathbf{F} = \mathbf{K}\mathbf{U}$ in Equation (1), the finite element analysis is carried out to solve the global displacement.

Finally, a sensitivity analysis of design variables is performed. Since $\mathbf{k}_e(\theta)$ contains only one variable θ , the sensitivities of compliance C to unit density and fiber angle $\frac{\partial C}{\partial x_e}$, $\frac{\partial C}{\partial \theta_e}$ are as follows:

$$\begin{cases} \frac{\partial C}{\partial x_e} = -p(x_e)^{p-1} \mathbf{u}_e^T \mathbf{k}_e(\theta) \mathbf{u}_e \\ \frac{\partial C}{\partial \theta_e} = -(x_e)^p \mathbf{u}_e^T \frac{\partial \mathbf{k}_e(\theta)}{\partial \theta_e} \mathbf{u}_e \end{cases}, \tag{6}$$

where \mathbf{u}_e is the element displacement matrix and $\frac{\partial \mathbf{k}_e(\theta)}{\partial \theta_e}$ is the sensitivity of the element stiffness matrix to the fiber angle of the element. $\frac{\partial \mathbf{k}_e(\theta)}{\partial \theta_e}$ is calculated as

$$\frac{\partial \mathbf{k}_e(\theta)}{\partial \theta_e} = \iint \frac{\partial \mathbf{k}_e(\theta_e)}{\partial \theta_e} \mathbf{B} dx dy = \iint \mathbf{B}^T \left(\frac{\partial \mathbf{T}}{\partial \theta_e} \mathbf{C} (\mathbf{T}^{-1})^T + \mathbf{T} \mathbf{C} \frac{\partial (\mathbf{T}^{-1})^T}{\partial \theta_e} \right) \mathbf{B} dx dy, \tag{7}$$

2.2. Solution Algorithm Considering Fiber Angle Constraint

In updating the element density, we refer to the optimization criterion method (OC) proposed by Sigmund. Taking the minimum structural compliance as the goal, the volume fraction is used as the constraint condition to solve the problem, which is convenient and efficient. In the fiber angle update, considering its nonlinear and multi-constrained objective function, this paper uses the moving asymptote method (MMA) to solve the problem.

While using the MMA to solve the fiber angle, the fiber angle constraint function is introduced. The fiber angle constraint function $f(\theta_e)$ in Equation (1) is defined as follows:

$$f(\theta_e) = \begin{cases} 0 & \text{FCR} \geq \text{fcr} \\ \text{FCR} - \text{fcr} & \text{FCR} < \text{fcr} \end{cases} \quad (8)$$

where θ_e represents the fiber angle of unit e and changes in $[0, 1]$ and the FCR and fcr are the fiber continuity rate of the current iteration result and the predefined fiber continuity rate, respectively.

When $\text{FCR} \geq \text{fcr}$, the fiber continuity rate of the current iteration results meets the requirements, without constraints, and the function value is 0. When $\text{FCR} < \text{fcr}$, the constraint is performed.

Figure 1 shows the schematic diagram of the fiber continuity ratio (FCR) calculation, and the equation is as follows:

$$\text{FCR} = \frac{\sum_{e=1}^{\text{nelx} \times \text{nely}} \left(\sum_{q=1}^{N_e} \cos \varphi_{e,q} \right)}{\sum_{e=1}^{\text{nelx} \times \text{nely}} N_e} \quad (9)$$

where φ_q is the angle of the q th adjacent element around the central element e and $\varphi_{e,q}$ is the difference between θ_e and $\alpha_{e,q}$. Then, use the cosine adjustment function to normalize $\varphi_{e,q}$, where N_e is the number of neighborhood units, nelx is the number of unit columns, and nely is the number of unit rows, as shown in Figure 1.

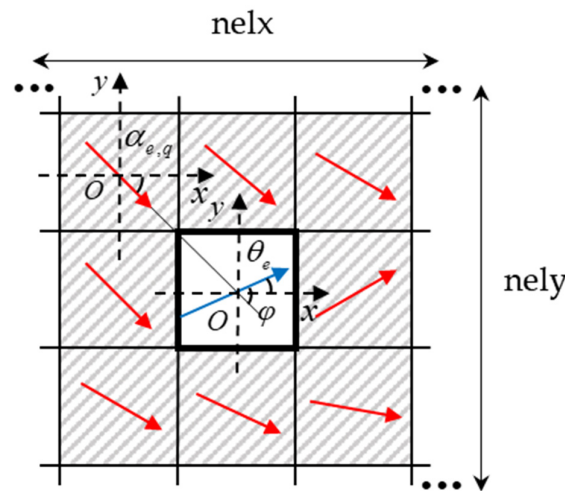


Figure 1. Schematic diagram of the calculation method for the fiber continuity ratio (FCR).

Since the design variable θ_e changes freely in the range of $[-\frac{\pi}{2}, \frac{\pi}{2}]$, the value range of $\varphi_{e,q}$ is $[0, \pi]$. Since we quantify the degree of continuity of the fiber by the accumulation and normalization of the cosine value of $\varphi_{e,q}$, the cosine value of $\varphi_{e,q}$ has a non-negative requirement, and it is necessary to adjust $\varphi_{e,q}$ in segments, as shown in Figure 2.

The angle adjustment method shown in Figure 2 is scientific because the degree of fiber continuity represented by $\varphi_{e,q}$ and $\pi - \varphi_{e,q}$ is the same, and we only make corresponding adjustments for the difference in the cosine values of the two. Subsequently, $\varphi_{e,q}$ is calculated according to the segmentation method as follows:

$$\varphi_{e,q} = \begin{cases} \theta_e - \alpha_{e,q} & |\theta_e - \alpha_{e,q}| \leq \frac{\pi}{2} \\ \pi - (\theta_e - \alpha_{e,q}) & |\theta_e - \alpha_{e,q}| > \frac{\pi}{2} \end{cases} \quad (10)$$

where θ_q is the fiber angle of the q th unit in the neighborhood of θ_e .

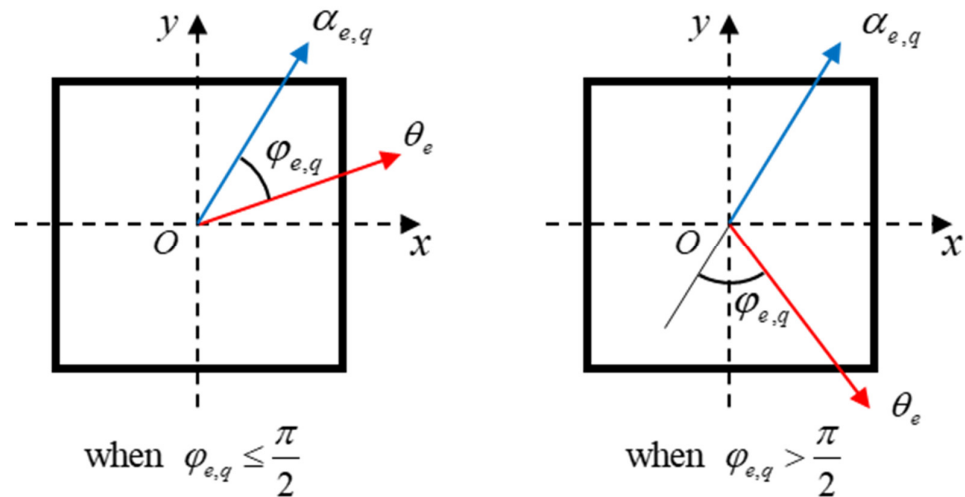


Figure 2. Adjustment of the fiber angle difference $\varphi_{e,q}$ between adjacent units.

On this basis, it is also necessary to calculate the gradient value of the constraint function to the design variable to meet the correct search direction of the constraint condition. The gradient value $df(\theta_e)$ of the constraint function $f(\theta_e)$ to all element fiber angles θ_e is calculated in Equations (8)–(10) as follows:

$$df(\theta_e) = \begin{cases} 0 & \text{FCR} \geq \text{fcr} \\ \sum_{q=1}^{N_e} [\sin(\theta_e - \alpha_{e,q}) \cdot \varphi_{e,q}'] & \text{FCR} < \text{fcr} \end{cases} \quad (11)$$

where $\varphi_{e,q}'$ is the derivative of $\varphi_{e,q}$ to θ_e , which is calculated as follows:

$$\varphi_{e,q}' = \begin{cases} 1 & |\theta_e - \alpha_{e,q}| \leq \frac{\pi}{2} \\ -1 & |\theta_e - \alpha_{e,q}| > \frac{\pi}{2} \end{cases} \quad (12)$$

2.3. Adaptive Filtering of the Fiber Angle

In the method of concurrent optimization of topology and fiber angle, many scholars have not filtered the fiber angle, which leads to poor continuity of the fiber; in addition, the traditional filtering method uses a distance-weighted filter to adjust the fiber angle. This filtering scheme will lead to excessive smoothing of the fiber, thereby reducing the stiffness of the overall structure. Therefore, this section proposes an adaptive filtering method for the fiber angle. This method uses the characteristics of the Gaussian function to dynamically adjust the filtering strength according to the real-time optimization effect and then moderately smooth the fiber angle. Since the introduction of the constraint function in Section 2.2 improves the continuity of the fiber, but at the same time leads to a decrease in the overall structural stiffness, the role of adaptive filtering is to ensure the continuity of the fiber while improving the stiffness of the overall structure.

Firstly, the traditional filtering methods are reviewed as follows:

$$\hat{t}_e = \frac{\sum_{m=1}^N \hat{H}_m t_m}{\sum_{m=1}^N \hat{H}_m} \quad (13)$$

where \hat{t}_e is the fiber angle of the central unit after filtration; t_m is the fiber angle of the neighborhood of the central unit before filtering; N is the number of neighborhood units; and \hat{H}_m is the weight factor, which is defined as follows:

$$\hat{H}_m = r_{\min} - \text{dist}(e, m), \{m \in N, |\text{dist}(e, m)| \leq r_{\min}\}, \tag{14}$$

where $\text{dist}(e, m)$ is the distance between unit m and central unit e and r_{\min} is the filter radius.

The adaptive filtering of fiber angle is based on the characteristics of the Gaussian function. According to the convergence degree of fiber angle, the standard deviation of the Gaussian function is corrected in real time, and then the filtering strength is adjusted.

The convergence degree of the fiber angle is described by the maximum change value $\Delta\theta_{\max}$ of the design variable. The specific calculation is as follows:

$$\Delta\theta_{\max} = \max\{\theta_{n-1} - \theta_{n-2}\}, \tag{15}$$

where n represents the number of iterations and $\theta_{n-1}, \theta_{n-2}$ are the fiber angle values of all elements in this iteration and the previous iteration results, respectively.

Figure 3 is the calculation diagram of $\theta_{n-1}, \theta_{n-2}$. The difference between the fiber angles of all units in the two iteration results is calculated, and the maximum difference is selected as $\Delta\theta_{\max}$, which indicates the convergence degree of fiber angle optimization. It is also used as a correction factor for the standard deviation $\hat{\sigma}_\theta$ of the Gaussian function for the real-time correction of fiber angle filtering. The modified equation is as follows:

$$\hat{\sigma}_\theta = \Delta\theta_{\max} \cdot \sigma_\theta, \tag{16}$$

Here, $\hat{\sigma}_\theta$ is the standard deviation of the modified Gaussian function and σ_θ is the initial value of the predefined standard deviation.

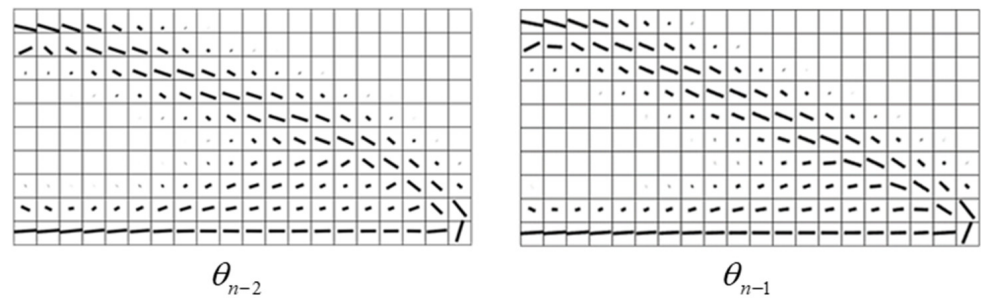


Figure 3. The fiber angle distribution of the n th and $(n - 1)$ th iterations.

After correcting the standard deviation of the Gaussian function, the weight of the Gaussian kernel function is calculated as follows:

$$W_\theta(r_z) = \frac{1}{2\pi\hat{\sigma}_\theta^2} e^{-\frac{r_z^2}{2\hat{\sigma}_\theta^2}}, r_z \leq r_{\min}, \tag{17}$$

where W_θ is the Gaussian kernel function used for fiber angle filtering and r_z is the distance between all units in the filtering area and the central unit.

The size of the standard deviation $\hat{\sigma}_\theta$ can determine the degree of influence of the surrounding units on the central unit in the filtering area. The larger the standard deviation, the greater the influence of the surrounding units on the central unit, and the more obvious the filtering effect. On the contrary, the filtering effect is weaker.

In order to intuitively feel the influence of the standard deviation of different Gaussian functions on the weights, Figure 4 shows the filter function image and the weight distribution of each unit in the filter area when the filter radius $\hat{\sigma}_\theta$ is 0.5, 1, and 5, respectively. The gray value corresponds to the size of the weight. These 3×3 grids are the fiber angle filters determined by the Gaussian function.

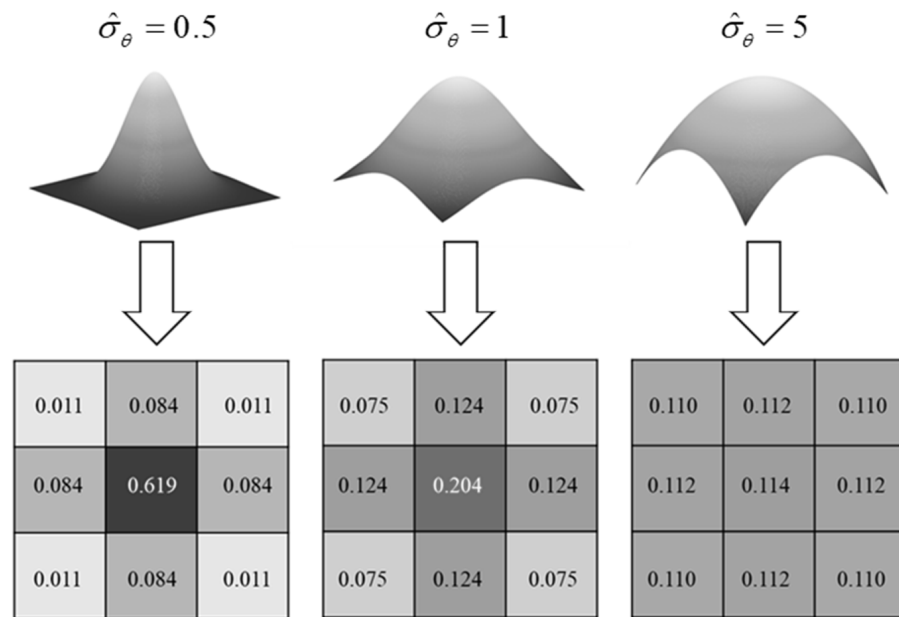


Figure 4. Gaussian function image and its corresponding normalized weight distribution.

Finally, the Gaussian kernel function in the filtering area is normalized, and the filtering of the fiber angle is completed. The specific equation is as follows:

$$\hat{\theta}_e = \sum_e \left(\frac{W_\theta(r_z)}{\sum_{z \in N_e} W_\theta(r_z)} \cdot \theta_e \right), \tag{18}$$

where $\hat{\theta}_e$, θ_e are the fiber angles before and after filtration, respectively.

In fiber angle filtering, the advantage of adaptive filtering over traditional filtering is that it can adjust the filtering parameters in real time according to the current optimization status and objectives to ensure the continuity and rationality of the fiber angle distribution. The adjustment of the standard deviation makes the filter more strongly smooth the fiber angle distribution when needed, while at other times, it can maintain a weak smoothing effect to avoid performance loss caused by excessive smoothing.

In summary, the adaptive filtering of the fiber angle effectively balances the relationship between the fiber continuity rate and the overall structural stiffness, which ensures fiber continuity while obtaining a more reasonable fiber angle distribution, thereby improving the overall structural stiffness. This provides an efficient, flexible, and robust method for fiber angle optimization, which can optimize structural performance while satisfying the design constraints.

2.4. Optimization Sequence

In the density-based concurrent optimization framework, combined with the fiber angle constraint strategy and adaptive filtering technology, a more reasonable fiber angle can be adjusted on the basis of improving fiber continuity, thereby ensuring overall structural stiffness.

Figure 5 is the specific optimization process of the method. Firstly, the parameters and variables are initialized, the element stiffness matrix is calculated, and the finite element analysis is carried out. Then, after the unit density sensitivity filtering, the OC method is used to update the unit density. At the same time, the fiber angle is adaptively filtered to calculate the maximum change value of the fiber angle so as to update the standard deviation of the Gaussian function. After using the Gaussian function to smooth the fiber angle, the MMA algorithm that fuses the fiber angle constraint function is used to complete the update of the fiber angle. Finally, the iterative element density and fiber angle are

output. The convergence condition is that the change value of the design variables is less than 0.01, and the optimization is completed if the convergence condition is satisfied. Otherwise, the calculation step of the element stiffness matrix is returned to continue the iteration.

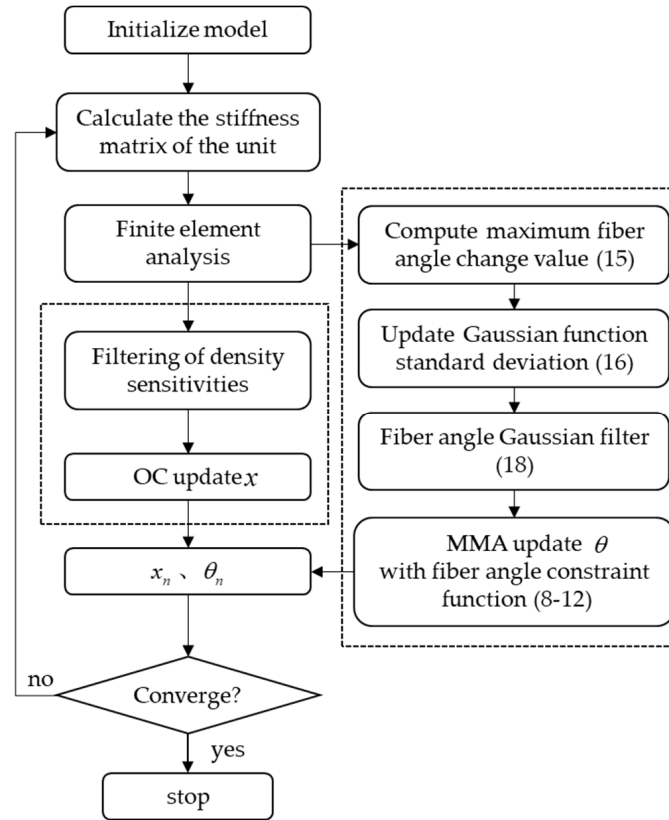


Figure 5. Topology optimization flowchart of anisotropic materials with smooth fiber orientation.

3. Numerical Results

In this section, based on the fiber angle constraint strategy and adaptive filtering technology, the topology optimization results of anisotropic materials with smooth fiber orientation are optimized by MATLAB (see Appendix A). After completing the boundary condition setting, through a series of numerical examples, the optimization results are compared and verified from the three perspectives of fiber continuity, overall structural stiffness, and numerical stability, and then the effectiveness and stability of the method are illustrated.

3.1. Parameters and Boundary Conditions

In this paper, the single-layer graphite/epoxy material with 70% fiber content is used as the optimization object, and the engineering material constants are shown in Table 1.

Table 1. Engineering elastic constants of single-layer graphite/epoxy composites with 70% fiber content.

Material	Mode	$E_1/10^5$ MPa	$E_2/10^5$ MPa	ν_{12}	$G_{12}/10^5$ MPa
graphite/epoxy	T300/5280	185	10.5	0.28	7.3

This section presents six boundary conditions to be optimized, as shown in Figure 6. Among them, (a) is a cantilever beam with a length–width ratio of 2:1. The left end of the structure is fixed, and the lower part of the right end is subjected to a downward concentrated load. (b) Is a double-load cantilever beam with a length–width ratio of 2:1. The left end of the structure is fixed, and the upper and lower parts of the right end

bear a downward concentrated load, respectively. (c) Is a double-hole cantilever beam with a length–width ratio of 2:1. Two holes are set in the design domain. The left end of the structure is fixed, and the lower part of the right end is subjected to a downward concentrated load. (d) Is a bridge girder with a length–width ratio of 4:1. The left and right sides are the supporting points, and the middle and lower parts bear the downward concentrated load. (e) Is a double-load bridge beam with a length–width ratio of 2:1. The left and right sides are the supporting points, and the bottom 1/3 and 2/3 are subjected to downward concentrated load, respectively. (f) Is an L-shaped beam whose shape is equivalent to removing a rectangle with a length–width ratio of 1:2 from the upper right of a rectangle with a length–width ratio of 2:3. The upper end is fixed, and the middle of the right end is subjected to a downward concentrated load.

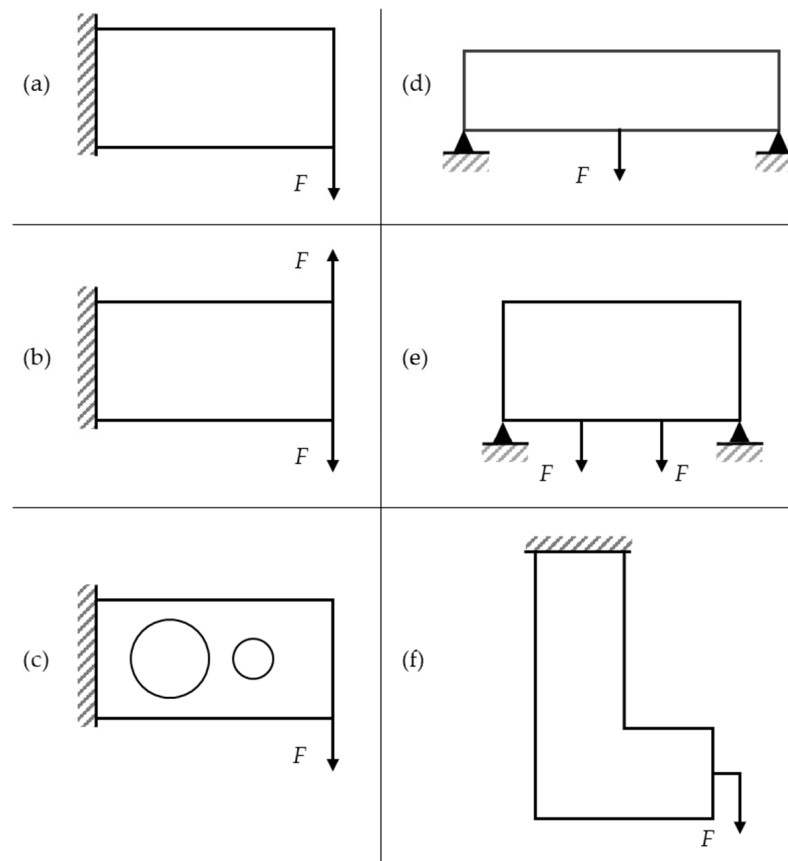


Figure 6. Boundary conditions: (a) cantilever beam; (b) double-load cantilever beam; (c) double-hole cantilever beam; (d) bridge girder; (e) double-load bridge beam; (f) L-shaped beam.

According to the different boundary conditions, the code can be freely adjusted. For example, in the optimization of the bridge beam, the numerical values of nel_x , $nely$, $penal$, $rmin$, $angle$, $volfrac$, sig_x , sig_t , and the fcr are set to 80, 20, 3, 1.5, $\pi/2$, 0.3, 5, 20, and 0.98, respectively.

3.2. Analysis of Structural Stiffness and Fiber Continuity

In this section, according to the boundary conditions set in Section 3.1, three schemes are used for optimization. Scheme (1) does not consider the fiber angle constraint and uses the traditional filtering method; scheme (2) considers the fiber angle constraint and uses the traditional filtering method; and scheme (3) considers the fiber angle constraint and uses the adaptive filtering method. Figure 7 shows the optimization results and data of each boundary condition under different schemes. The data are the overall structural compliance and the fiber continuity rate, which are represented by C and FCR , respectively. Among them, the compliance is the reciprocal of the stiffness, and the smaller the compliance, the greater

the stiffness. The structural compliance and fiber continuity of all the results in Figure 7 are calculated using the histogram in Figures 8 and 9, respectively, which is convenient for data comparison and analysis of different optimization schemes. Figures 10 and 11, respectively, present the topological structure and fiber angle distribution, fiber continuity trend, and structural compliance trend of the double-load cantilever beam in Figure 7. Similarly, Figures 12–14 show the topological structure and fiber angle distribution of the bridge beam in Figure 7, the changing trend of the fiber continuity rate, and the changing trend of structural compliance.

	(1) Without constraint & Traditional filter	(2) With constraint & Traditional filter	(3) With constraint & Adaptive filter
(a)	 (a-1) C: 73.96 FCR: 90.05%	 (a-2) C: 75.72 FCR: 98.04%	 (a-3) C: 74.30 FCR: 98.73%
(b)	 (b-1) C: 177.36 FCR: 83.70%	 (b-2) C: 247.91 FCR: 98.04%	 (b-3) C: 197.11 FCR: 97.94%
(c)	 (c-1) C: 91.14 FCR: 81.53%	 (c-2) C: 120.64 FCR: 97.99%	 (c-3) C: 116.40 FCR: 99.31%
(d)	 (d-1) C: 19.75 FCR: 85.82%	 (d-2) C: 54.30 FCR: 98.05%	 (d-3) C: 26.76 FCR: 98.01%
(e)	 (e-1) C: 42.08 FCR: 81.07%	 (e-2) C: 74.00 FCR: 98.02%	 (e-3) C: 66.19 FCR: 98.00%
(f)	 (f-1) C: 121.01 FCR: 85.94%	 (f-2) C: 165.84 FCR: 98.03%	 (f-3) C: 153.38 FCR: 98.03%

Figure 7. Concurrent optimization results of different schemes for each boundary condition. (a–f) Correspond to the six boundary conditions in Figure 6, respectively, and the fcr (predefined fiber continuity constraint) of schemes (2) and (3) is set to 0.98.

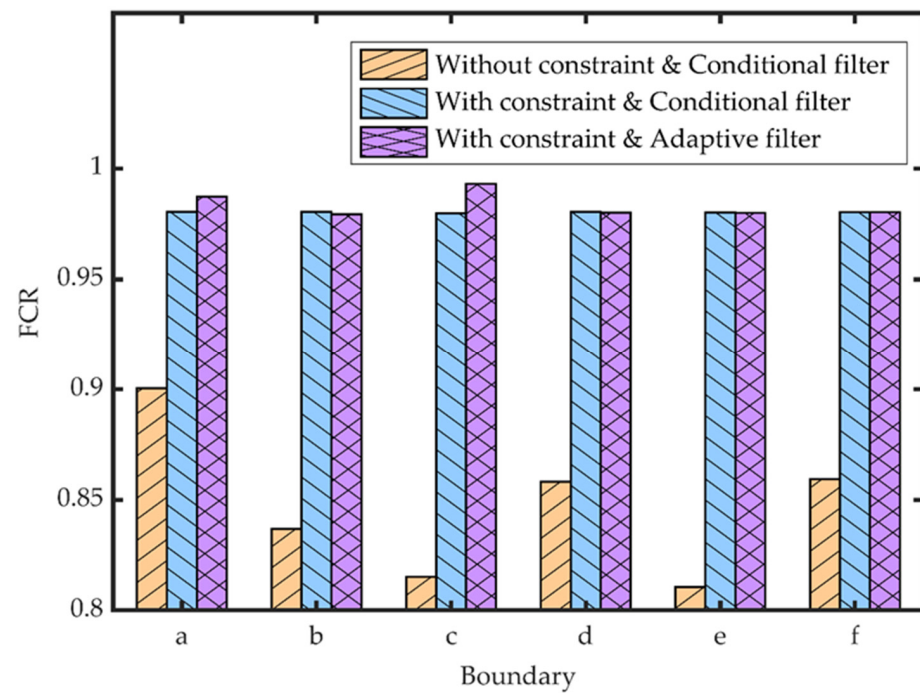


Figure 8. Comparison of the fiber continuity rates of different optimization schemes under different boundary conditions (a–f) Correspond to the six boundary conditions in Figure 6, respectively.

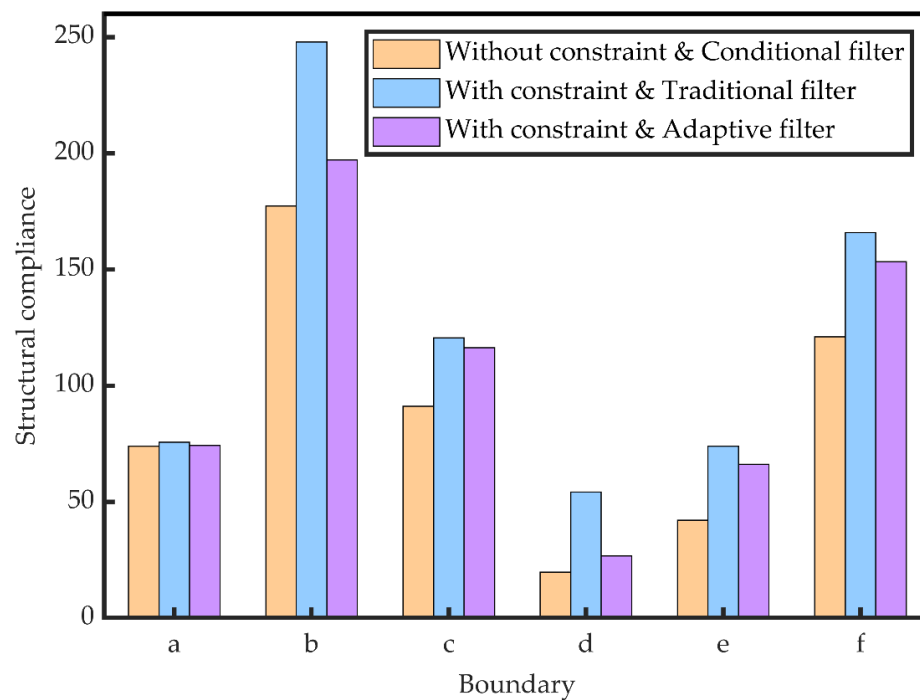


Figure 9. Comparison of structural compliance of different optimization schemes under different boundary conditions (a–f) Correspond to the six boundary conditions in Figure 6, respectively.

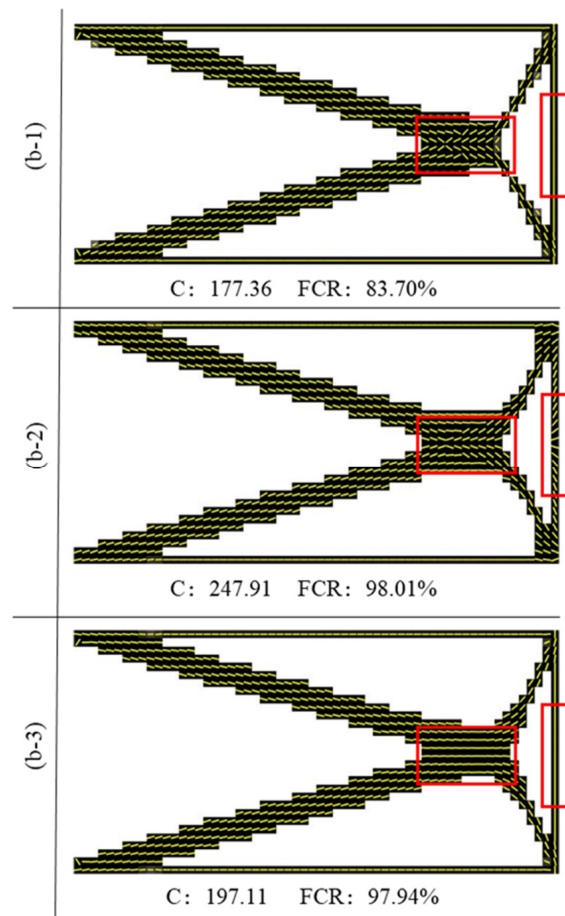


Figure 10. The optimization results of the double-load cantilever beam with different schemes correspond to the results of (b-1–b-3) in Figure 7, which shows a detailed analysis.

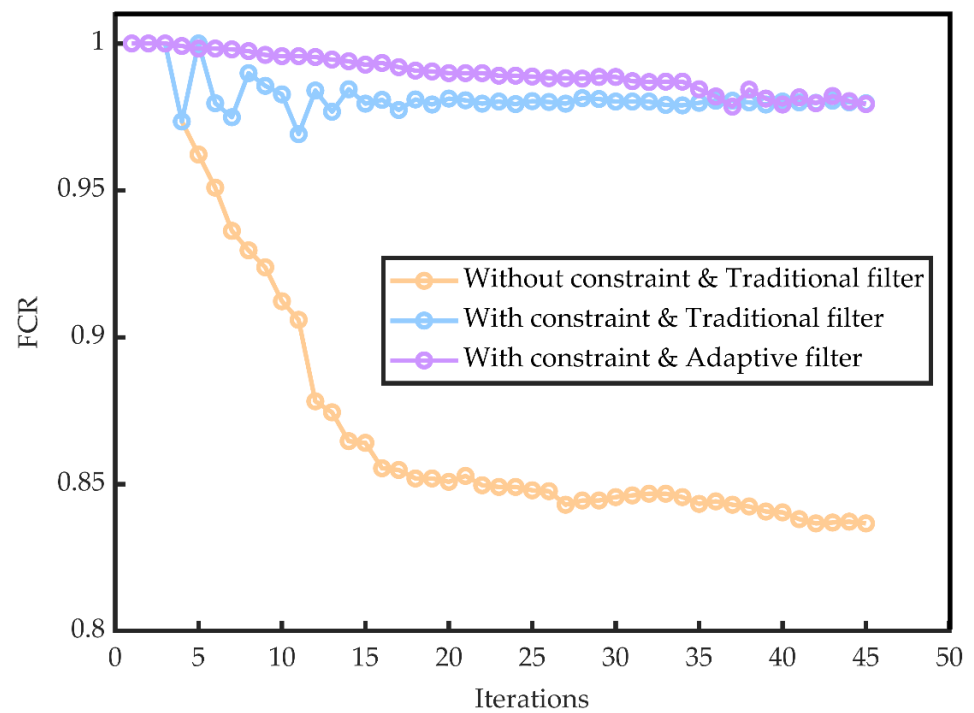


Figure 11. Trend of the fiber continuity rate of the double-load cantilever beam with different schemes.

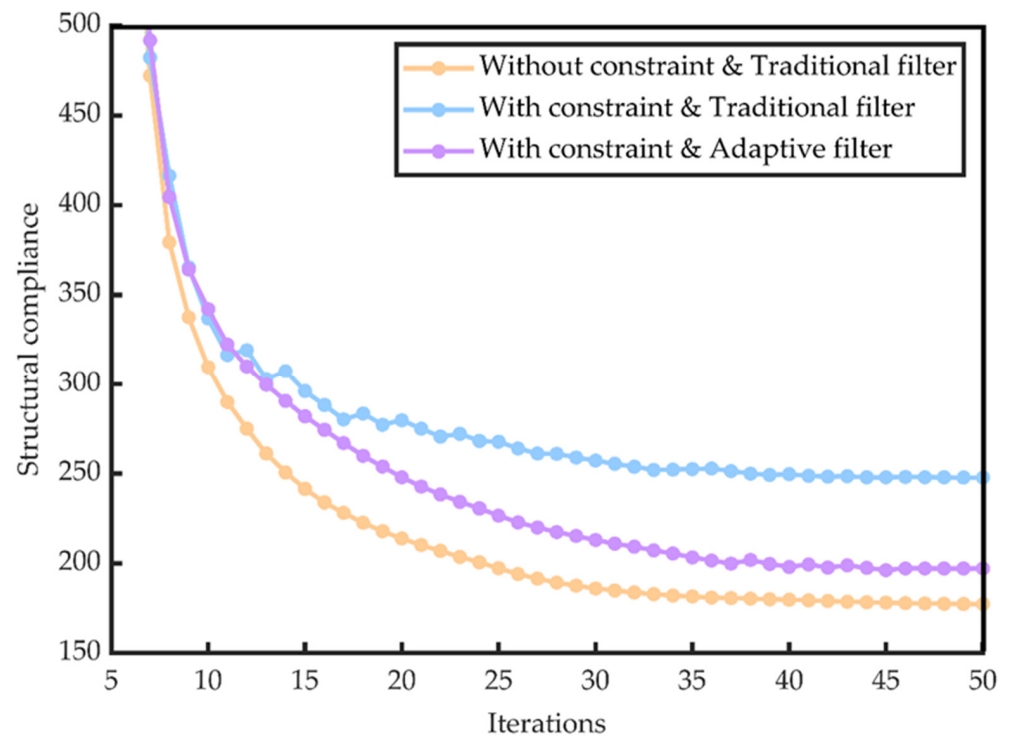


Figure 12. Trend of structural compliance of the double-load cantilever beam with different schemes.

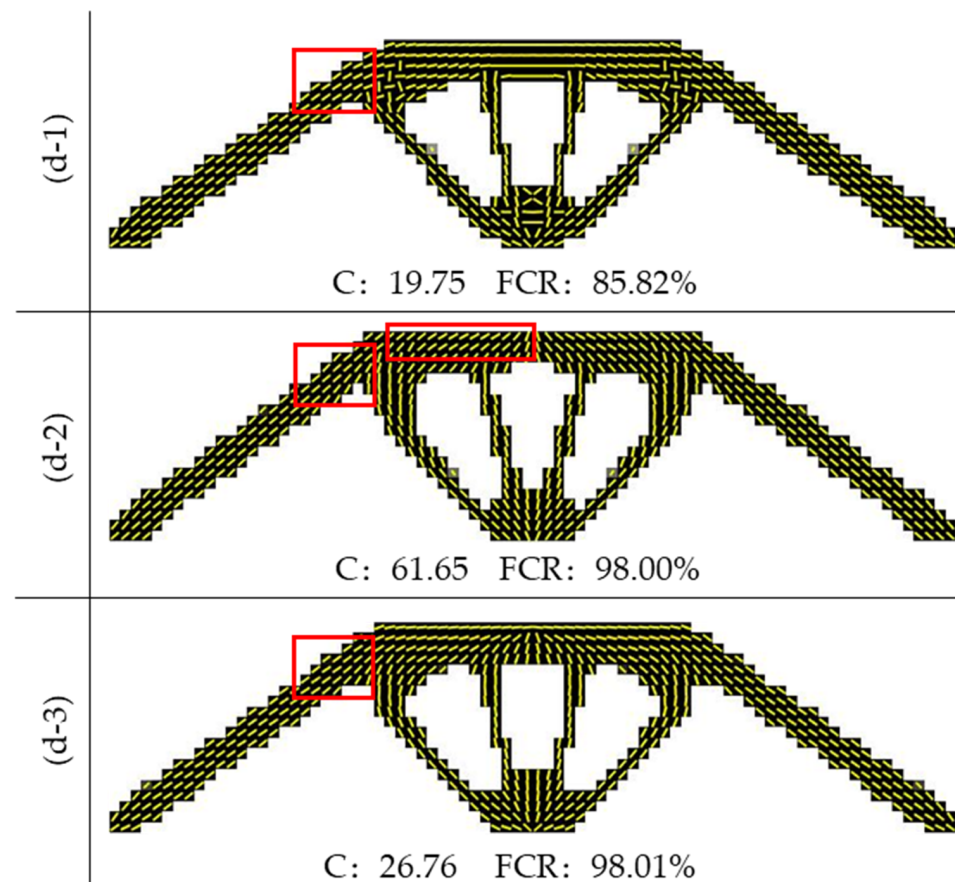


Figure 13. The optimization results of different schemes are adopted for the bridge girder, corresponding to the results of (d-1–d-3) in Figure 7, which shows a detailed analysis.

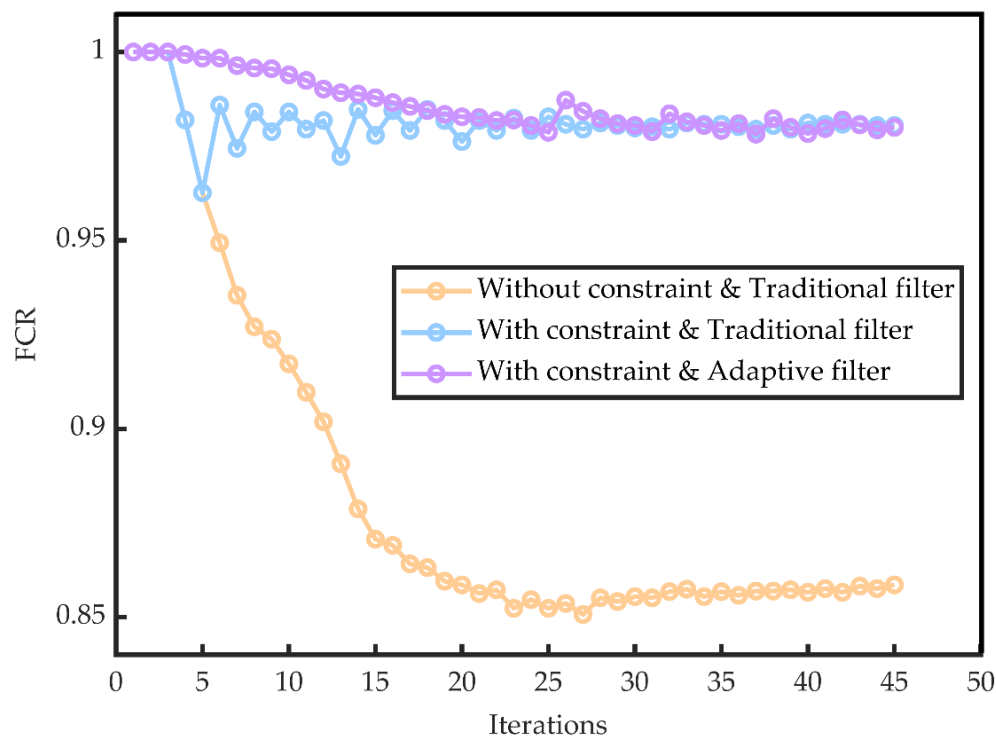


Figure 14. Trend of the fiber continuity rate of the bridge girder with different schemes.

As shown in Figure 7, the six examples are analyzed from the data. The structural compliance of scheme (1) is small, but the fiber continuity rate is low. After considering the fiber angle constraint, that is, scheme (2), the fiber continuity rate is significantly improved, which can be maintained at about 98%, but the compliance is greatly increased; on the basis of considering the fiber angle constraint, the adaptive filter is introduced, that is, scheme (3). The fiber continuity rate is still maintained at about 98%, or even higher, and the structural compliance is also greatly reduced compared with scheme (2). This means that the concurrent optimization method combining the fiber angle constraint strategy and the adaptive filtering technology is effective. It not only improves the fiber continuity rate but also ensures the overall structural stiffness to a certain extent.

Figure 8 intuitively shows the comparison of fiber continuity with different optimization schemes under different boundary conditions. After the fiber angle constraint, the fiber continuity rate increased significantly to about 98%. Furthermore, after introducing the adaptive filtering technology on the basis of the fiber angle constraint, the fiber continuity rate is still maintained at about 98% or even higher.

Figure 9 intuitively shows the structural compliance comparison of different optimization schemes under different boundary conditions. After the fiber angle constraint, the compliance increases significantly, indicating that while improving fiber continuity, the overall structure's resistance to force decreases significantly, and the mechanical properties deteriorate. After the further introduction of adaptive filtering technology, we observed a significant decrease in structural compliance, which indicates that the mechanical properties have been improved to a certain extent. Although the compliance at this time is still slightly higher than the level in scheme (1), in the process of pursuing fiber continuity, the original optimal fiber angle distribution must be adjusted. This adjustment will inevitably affect the mechanical properties of the structure to a certain extent. Our design goal is to ensure that fiber continuity is improved while minimizing the sacrifice of the overall structural stiffness. Scheme (3) is based on this goal. By combining the fiber angle constraint strategy and adaptive filtering technology, the structural stiffness is maintained to the greatest extent while improving fiber continuity so as to achieve the purpose of optimization.

Combined with the analysis of Figures 8 and 9, it is concluded that adaptive filtering can maintain the continuity of fibers. Its more prominent advantage is that compared with the optimization scheme without adaptive filtering, it optimizes the topology with higher stiffness, which is the embodiment of both manufacturability and mechanical properties.

Figure 10 shows the optimization results of the boundary conditions of the double-load cantilever beam with different schemes. It is a diagram enlarged by the results of (b-1), (b-2), and (b-3) in Figure 7, which is intended to analyze the differences in topology and fiber angle distribution. From the perspective of fiber angle distribution, the angle in scheme (1) is discontinuous, especially at the node and support of the bar, and the fiber angle of the adjacent unit has a sudden change, so the fiber continuity rate is low—only 83.70%. In scheme (2), the angle is continuous, and there is no sudden change in the angle of the fiber at the node and the support of the bar. However, in the vertical bar at the rightmost end, the fiber angle shows an inconsistent distribution with the direction of the bar, resulting in poor mechanical properties, which is also the result of the forced constraint of the fiber angle. In scheme (3), the fiber angle continuity is higher and it is consistent with the direction of the bar, and the structural stiffness is higher.

From the topological point of view, the results of the three schemes are roughly the same. The two inclined rods at the right end of schemes (2) and (3) are more curved, which is affected by the adjusted fiber angle in concurrent optimization.

From the perspective of structural compliance, the compliance of the three schemes is 177.36, 247.91, and 197.11, respectively. The compliance of scheme (2) is about 33% higher than that of scheme (1), indicating that the stiffness decreases. The compliance of scheme (3) is 20% lower than that of scheme (2), and the overall stiffness is greatly increased.

Figure 11 shows a comparison of the trend of fiber continuity under different optimization schemes. In the diagram, it can be seen that scheme (1) is not affected by constraints and gradually converges to 83.70% in concurrent optimization; scheme (2) began to introduce constraints at the fifth iteration, and the fiber continuity rate increased significantly, began to fluctuate, and finally converged to 98%. Scheme (3) introduces constraints at the beginning of the 34th iteration, and the fluctuation is small and finally converges at 98%.

Figure 12 shows a comparison of the structural compliance change trend of the double-load cantilever beam under different optimization schemes. In the diagram, it can be seen that scheme (1) is not affected by constraints, the compliance eventually converges to 177.36, and the overall structural stiffness is large; the compliance of scheme (2) fluctuates greatly and finally converges to 247.91, and the overall structural stiffness is small. The compliance fluctuation of scheme (3) is very small, converging to 197.11, and the structural stiffness is greatly improved compared with scheme (2).

Similar to Figure 10, Figure 11 presents the optimization results of the bridge girder with different schemes, which is the enlarged structure diagram of (d-1), (d-2), and (d-3) in Figure 7. From the perspective of fiber angle distribution, fiber continuity of scheme (1) is poor, only 85.82%; the angle of scheme (2) is relatively continuous, and there is no sudden change in the angle of the fiber at the node and the support of the bar. However, in the horizontal bar at the top end, the fiber angle shows an inconsistent distribution with the direction of the bar, resulting in poor mechanical properties, which is also the result of the forced constraint of the fiber angle. In scheme (3), fiber angle continuity is higher and it is consistent with the direction of the bar, and the structural stiffness is higher.

From the perspective of topology, the three schemes are roughly the same, and the structure contour of scheme (3) is smoother because it is affected by the adjusted fiber angle in concurrent optimization.

From the perspective of structural compliance, the compliance of the three schemes is 19.75, 61.65, and 27.96, respectively. The compliance of scheme (2) is about 214% higher than that of scheme (1), and the stiffness is lower. The compliance of the results of scheme (3) is 55% lower than that of scheme (2), and the overall stiffness is greatly increased.

Figure 14 shows the variation trend of the fiber continuity rate of the bridge girder with different optimization schemes. In the diagram, it can be seen that scheme (1) is not affected

by constraints and gradually converges to 85.82% in concurrent optimization; scheme (2) introduced constraints at the sixth iteration, and the fiber continuity rate increased significantly, began to fluctuate, and finally converged to 98.00%. Scheme (3) introduces constraints at the beginning of the 34th iteration, and the fluctuation is small. Finally, it also converges at 98.01%.

Figure 15 shows the changing trend of the structural compliance of bridge girders with different optimization schemes. In the diagram, it can be seen that scheme (1) is not affected by constraints, the compliance eventually converges to 19.75, and the overall structural stiffness is large; the compliance change in scheme (2) fluctuates greatly and finally converges to 61.65, and the overall structural stiffness is small. The compliance fluctuation of scheme (3) is very small, converging to 27.96, and the structural stiffness is greatly improved compared with scheme (2).

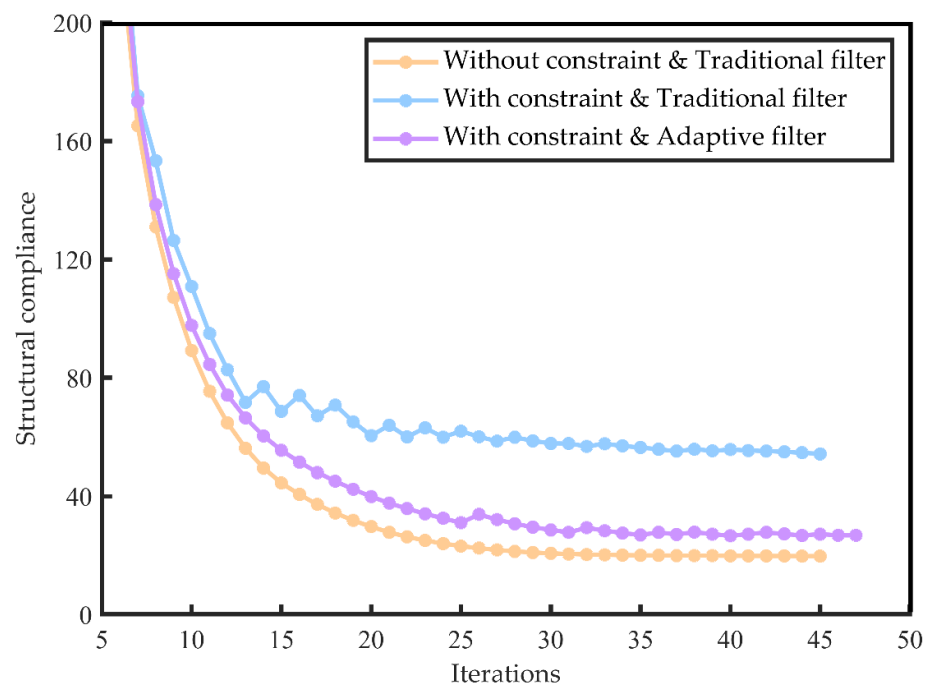


Figure 15. Trend of the structural compliance of the bridge girder with different schemes.

In summary, in the concurrent optimization considering fiber angle constraints, the results show a smoother fiber distribution. However, this mandatory constraint sacrifices the mechanical properties of the material to a certain extent, resulting in a decrease in the overall stiffness of the structure. In order to solve this problem, we introduce adaptive filtering technology on the basis of fiber angle constraints. Through the application of this technology, not only is the continuity of the fiber significantly improved but also the overall stiffness of the structure is effectively maintained, and the balance between the optimization goal and the mechanical properties is achieved.

3.3. Numerical Stability

Both Figures 16 and 17 show the concurrent optimization results of the cantilever beam and the double-load bridge beam at six grid resolutions. Under the two boundary conditions, the six topologies are roughly the same, but with the refinement of the mesh, the obtained material distribution is more accurate and the structural contour is smoother. The fiber orientation of all the results is basically consistent with the direction of the rod and maintains a high continuity and a relatively smooth distribution at the node of the rod.

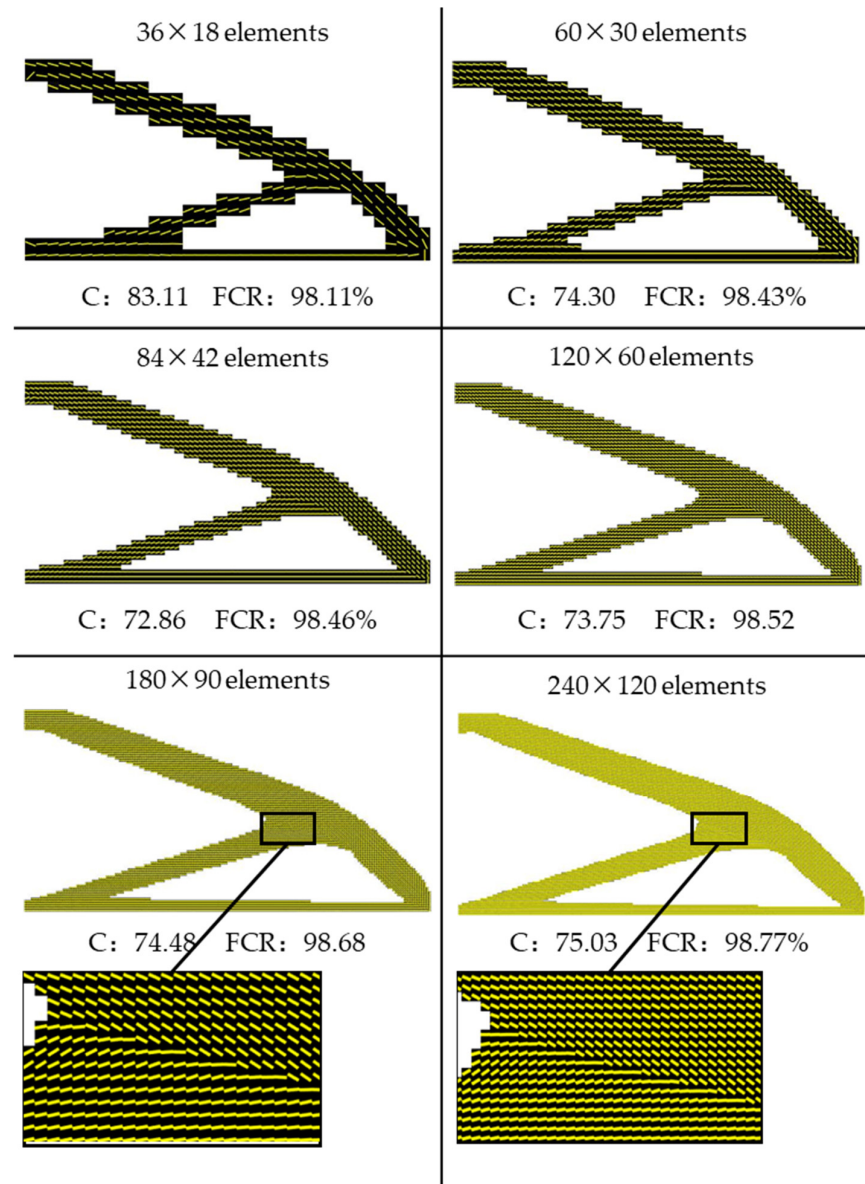


Figure 16. Concurrent optimization results of a cantilever beam under different grid divisions. The fcr was set to 0.98.

From the data in Figures 16 and 17, the fiber continuity rate of the final optimization results remained at a high level, and the fiber continuity rate remained at about 98% or even higher. The structural compliance decreases with the refinement of the grid and gradually tends to be stable. In the cantilever beam case, when the grid is divided into 36×18 , the compliance is 83.11, which is larger. When divided into denser grids, that is, 60×30 , 84×42 , 120×60 , 180×90 , and 240×120 , the compliance is smaller, 74.30, 72.86, 73.75, 74.48, and 75.03, respectively. In the case of the double-load cantilever beam, when the grid is divided into 36×18 and 60×30 units, the structural compliance is 103.38 and 66.20, respectively which is larger; when it is divided into denser grids, that is, 84×42 , 120×60 , 180×90 , and 240×120 , the compliance is 45.84, 38.25, 36.15, and 36.06, respectively.

From this point of view, the compliance decreases with the refinement of the mesh and gradually tends to be stable. The fiber continuity rate of all of the optimization results maintains a high level, which means the mesh independence of the method is high.

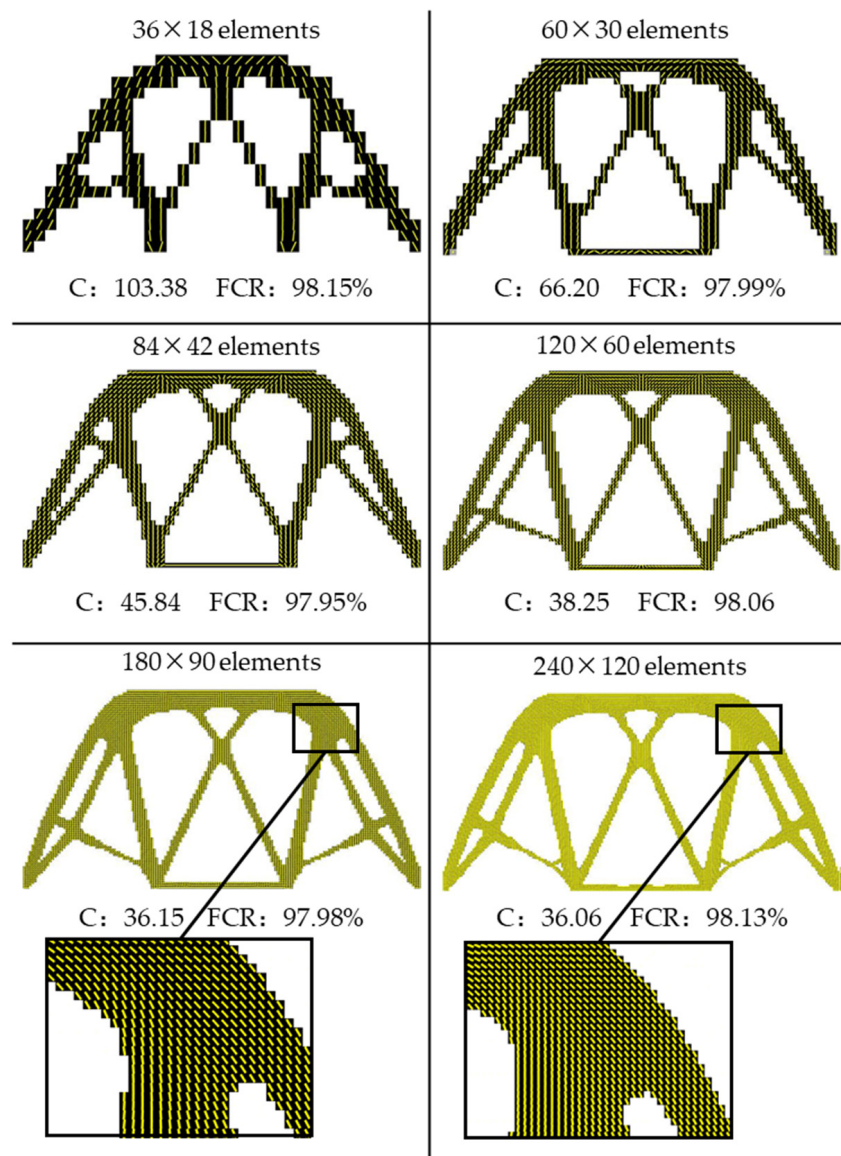


Figure 17. Concurrent optimization results of double-load bridge beams under different mesh divisions. The fcr was set to 0.98.

Figure 18 shows the concurrent optimization results of the cantilever beam, double-hole cantilever beam, and L-shaped beam under different volume constraints. In the optimization, the volume fraction is predefined as 0.3, 0.4, and 0.5, respectively, and the amount of constrained material is optimized concurrently. In the diagram, it can be seen that with the increase in volume fraction, the material stability in the design domain increases, and a reasonable optimization result is formed, the structural compliance decreases steadily, and the fiber continuity rate maintains a high level.

The comprehensive analysis shows that the topology optimization method of anisotropic materials with the smooth fiber orientation proposed in this paper performs well in numerical stability. On the one hand, the grid independence of the concurrent optimization method is high, that is, under different grid division conditions, the distribution of the material layout and fiber angle maintains good consistency. With the refinement of the mesh, the structural compliance gradually decreases and tends to be stable. On the other hand, under the constraints of different volume fractions, the method significantly improves the continuity of the fiber angle and can achieve a reasonable material distribution, thereby ensuring the stiffness of the overall structure. These results not only prove the numerical

Numerical examples show that the fiber angle constraint strategy significantly improves the continuity of the fiber but also sacrifices the overall structural stiffness. However, by introducing adaptive filtering technology, not only is the continuity of the fiber significantly improved but also the structural stiffness is guaranteed, and the effective balance between the two is achieved.

However, the concurrent optimization of topology and the fiber angle also faces serious initial dependence problems. The appropriate initial value of the fiber angle is very important so as to get rid of the risk of falling into the local optimum. In addition, the MATLAB program provided in the Appendix is written based on the logic of 99 lines of code, which has high readability, but the running speed is slow. Therefore, vectorization operation or different optimization algorithms can be used in subsequent research to improve the running speed. These studies are necessary to further improve the optimization in future work and provide a more efficient and reliable solution for the topology optimization design and manufacturing of composite materials.

Author Contributions: Conceptualization, X.P. and C.S.; methodology, S.J.; software, J.L.; validation, B.Y., C.S. and X.P.; formal analysis, J.L.; investigation, S.J.; resources, C.S.; data curation, X.P.; writing—original draft preparation, C.S.; writing—review and editing, C.S.; visualization, S.J.; supervision, S.J.; project administration, S.J.; funding acquisition, J.L. All authors have read and agreed to the published version of the manuscript.

Funding: This work was funded by the Ningbo Key Research and Development Program [grant number 2023Z134] and the Taizhou Science and Technology Plan Program [23GYB37].

Institutional Review Board Statement: Not applicable.

Informed Consent Statement: Not applicable.

Data Availability Statement: The data used to support the findings of this study are available within the article.

Conflicts of Interest: The authors declare no conflicts of interest.

Appendix A

```
function fiber_top(nelx,nely,penal,rmin,angle,volfrac,sig_x,sig_t,fcn)
x(1:nely,1:nelx)=volfrac;
t(1:nely,1:nelx)=angle;
loop=[0,0];
change = [0.2,0.1];
m=1; n=nely*nelx; move=0.1;
low=zeros(nely,nelx); low=reshape(low,n,1);
upp=ones(nely,nelx); upp=pi.*upp; upp=reshape(upp,n,1);
xold1=zeros(n,1); xold2=zeros(n,1);
while max(change)>0.01 && loop(1)<200
    loop(1)=loop(1)+1;
    [k]=ke(nelx,nely,t);
    [dk]=dke(nelx,nely,t);
    [U]=FE(nelx,nely,x,penal,k);
    c=0.;
    for ely=1:nely
        for elx=1:nelx
            n1=(nely+1)*(nelx-elx)+ely;
            n2=(nely+1)*(nelx-elx+1)+ely;
            Ue=U([2*n1-1;2*n1;2*n2-1;2*n2;2*n2+1;2*n2+2;2*n1+1;2*n1+2],1);
            c=c+x(ely,elx)^penal*Ue'*k(ely,elx).KE*Ue;
            dc_x(ely,elx)=-penal*x(ely,elx)^(penal-1)*Ue'*k(ely,elx).KE*Ue;
            dc_t(ely,elx)=-x(ely,elx)^penal*Ue'*dk(ely,elx).dKE*Ue;
        end
    end
end
```

```

        end
    end
    [dc_x,g]=GSfilter_x(nelx,nely,x,rmin,dc_x,sig_x);
    [xnew]=oc_x(nelx,nely,x,volfrac,dc_x);
    change(1)=max(abs(xnew(:)-x(:)));
    x=xnew;
    if change(2)>0.01
        [t]=GSfilter_t(nelx,nely,rmin,t,change,sig_t);
        [FCR,df1]=fiber_constraint(nelx,nely,t,rmin);
        [t,change,xold1,xold2,low,upp,loop,move]=mma...
            (nelx,nely,change,loop,df1,t,fcr,FCR,...
            dc_t,c,move,angle,m,n,xold1,xold2,low,upp);
    end
    disp(['It.: ' sprintf( '%4i',loop)...
        ' Obj.: ' sprintf('%10.4f',c)...
        ' Vol.: ' sprintf('%6.3f',sum(sum(x))/(nelx*nely))...
        ' ch.: ' sprintf('%6.3f',change)...
        ' grey.: ' sprintf('%6.3f',g)...
        ' FCR.: ' sprintf('%6.3f',FCR)])
    colormap(gray);imagesc(-x);axis equal;axis tight;axis off;pause(1e-6);
    hold on
    a1=-reshape(t,nely,nelx);
    xMax=2*max(x(:));
    quiver(-cos(a1).*x/xMax,-sin(a1).*x/xMax,0,'y','LineWidth',1);
    quiver(cos(a1).*x/xMax,sin(a1).*x/xMax,0,'y','LineWidth',1);
    end
end
function [k]=ke(nelx,nely,t)
a=1/2;b=1/2;
E1=1.85; E2=0.105;
v12=0.0159; v21=0.28; G12=0.073;
C=[E1/(1-v12*v21),(v21*E2)/(1-v12*v21),0,...
    (v21*E2)/(1-v12*v21),E2/(1-v12*v21),0,...
    0,0,G12];
k(nely,nelx)=struct('KE',[ ]);
for elx=1:nelx
    for ely=1:nely
        T=[cos(t(ely,elx)).^2,    sin(t(ely,elx)).^2,...
            2*cos(t(ely,elx))*sin(t(ely,elx));...
            sin(t(ely,elx)).^2,    cos(t(ely,elx)).^2,...
            -2*cos(t(ely,elx))*sin(t(ely,elx));...
            -cos(t(ely,elx))*sin(t(ely,elx)),...
            cos(t(ely,elx))*sin(t(ely,elx)),...
            cos(t(ely,elx)).^2-sin(t(ely,elx)).^2];
        D=T\C/(T.);
        KE = elementMatVec2D(a, b, D);
        k(ely,elx).KE=KE;
    end
end
end
function [KE,Be] = elementMatVec2D(a, b, D)
GaussNodes = [-1/sqrt(3); 1/sqrt(3)]; GaussWeigh = [1 1];
L = [1 0 0 0; 0 0 0 1; 0 1 1 0]; KE = zeros(8,8);
for i = 1:length(GaussNodes)
    for j = 1:length(GaussNodes)

```

```

GN_x = GaussNodes(i); GN_y = GaussNodes(j);
dN_x = 1/4*[-(1-GN_x) (1-GN_x) (1+GN_x) -(1+GN_x)];
dN_y = 1/4*[-(1-GN_y) -(1+GN_y) (1+GN_y) (1-GN_y)];
J = [dN_x; dN_y]*[ a -a a; b b -b -b];
G = [inv(J) zeros(size(J)); zeros(size(J)) inv(J)];
dN(1,1:2:8) = dN_x; dN(2,1:2:8) = dN_y;
dN(3,2:2:8) = dN_x; dN(4,2:2:8) = dN_y;
Be = L*G*dN;
KE = KE + GaussWeigh(i)*GaussWeigh(j)*det(J)*Be'*D*Be;
end
end
end
function [dk]=dke(nelx,nely,t)
dk(nely,nelx)=struct('dKE',[]);
syms tt;
a=0.5; b=0.5;
E1=1.85; E2=0.105;
v12=0.0159; v21=0.28; G12=0.073;
C=[E1/(1-v12*v21),(v21*E2)/(1-v12*v21),0;. . .
(v21*E2)/(1-v12*v21),E2/(1-v12*v21),0;. . .
0,0,G12];
T=[cos(tt).^2,sin(tt).^2,2*cos(tt)*sin(tt);. . .
sin(tt).^2,cos(tt).^2,-2*cos(tt)*sin(tt);. . .
-cos(tt)*sin(tt),cos(tt)*sin(tt),cos(tt).^2-sin(tt).^2];
dT_ni=diff(inv(T),tt);
dT_ni_zhuan=diff(inv(T.'),tt);
D=dT_ni*C/(T.')+ T\C*dT_ni_zhuan;
mf = matlabFunction(D);
for elx=1:nelx
for ely=1:nely
cc=mf(t(ely,elx));
dKE = dk_elementMatVec2D(a, b, cc);
dk(ely,elx).dKE=dKE;
end
end
end
function dKE= dk_elementMatVec2D(a, b, cc)
GaussNodes = [-1/sqrt(3); 1/sqrt(3)]; GaussWeigh = [1 1];
L = [1 0 0 0; 0 0 0 1; 0 1 1 0]; dKE = zeros(8,8);
for i = 1:length(GaussNodes)
for j = 1:length(GaussNodes)
GN_x = GaussNodes(i); GN_y = GaussNodes(j);
dN_x = 1/4*[-(1-GN_x) (1-GN_x) (1+GN_x) -(1+GN_x)];
dN_y = 1/4*[-(1-GN_y) -(1+GN_y) (1+GN_y) (1-GN_y)];
J = [dN_x; dN_y]*[ -a a -a; -b -b b b];
G = [inv(J) zeros(size(J)); zeros(size(J)) inv(J)];
dN(1,1:2:8) = dN_x; dN(2,1:2:8) = dN_y;
dN(3,2:2:8) = dN_x; dN(4,2:2:8) = dN_y;
Be = L*G*dN;
dKE = dKE + GaussWeigh(i)*GaussWeigh(j)*det(J)*Be'*cc*Be;
end
end
end
function [U]=FE(nelx,nely,x,penal,k)
K=sparse(2*(nelx+1)*(nely+1),2*(nelx+1)*(nely+1));
F=sparse(2*(nely+1)*(nelx+1),1);
U=sparse(2*(nely+1)*(nelx+1),1);

```

```

for elx=1:nelx
    for ely=1:nely
        n1=(nely+1)*(nelx-elx)+ely;
        n2=(nely+1)*(nelx-elx+1)+ely;
        edof=[2*n1-1;2*n1;2*n2-1;2*n2;2*n2+1;2*n2+2;2*n1+1;2*n1+2];
        K(edof,edof)=K(edof,edof)+x(ely,elx)^penal*(k(ely,elx).KE);
    end
end
ip=(nely+1)*(nelx+2);
F(ip,1)=-1;
fixeddofs = [2*nely+1,2*nely+2,2*(nely+1)*(nelx+1)-1,2*(nely+1)*(nelx+1)];
alldofs = [1:2*(nely+1)*(nelx+1)];
freedofs = setdiff(alldofs,fixeddofs);
U(freedofs,:)=K(freedofs,freedofs)\F(freedofs,:);
U(fixeddofs,:)=0;
end
function [dcn,g]=GSfilter_x(nelx,nely,x,rmin,dc_x,sig_x)
q(1:nely,1:nelx)=0;
sum_q=0.;
dcn=zeros(nely,nelx);
for ely=1:nely
    for elx=1:nelx
        if x(ely,elx)>0.001 && x(ely,elx)<1
            q(ely,elx)=1;
        end
        sum_q=sum_q+q(ely,elx);
    end
end
g=sum_q/(nelx*nely);
sig_x=g*sig_x;
for i=1:nelx
    for j=1:nely
        sum=0.0;
        w=zeros(nely,nelx);
        for k=max(i-floor(rmin),1):min(i+floor(rmin),nelx)
            for l=max(j-floor(rmin),1):min(j+floor(rmin),nely)
                fac=sqrt((i-k)^2+(j-l)^2);
                w(l,k)=exp(-fac^2/(2*sig_x^2))/(2*pi*sig_x^2);
                sum=sum+w(l,k);
            end
        end
        for k=max(i-floor(rmin),1):min(i+floor(rmin),nelx)
            for l=max(j-floor(rmin),1):min(j+floor(rmin),nely)
                w(l,k)=w(l,k)/sum;
                dcn(j,i)=dcn(j,i)+w(l,k)*dc_x(l,k)*x(l,k);
            end
        end
    end
end
end
function [xnew]=oc_x(nelx,nely,x,volfrac,dc)
l1=0;
l2=100,000;
move=0.2;
while (l2-l1>1e-4)
    lmid=0.5*(l2+l1);
    xnew =max(0.001,max(x-move,min(1.,min(x+move,x.*sqrt(-dc./lmid)))));

```

```

        if sum(sum(xnew))-volfrac*nex*nely>0
            l1=lmid;
        else
            l2=lmid;
        end
    end
end
function [tnew]=GSfilter_t(nex,nely,rmin,t,change,sig_t)
sig_t=change(2)*sig_t;
tnew=zeros(nely,nex);
for i=1:nex
    for j=1:nely
        sum=0.0;
        w=zeros(nely,nex);
        for k=max(i-floor(rmin),1):min(i+floor(rmin),nex)
            for l=max(j-floor(rmin),1):min(j+floor(rmin),nely)
                fac=sqrt((i-k)^2+(j-l)^2);
                w(l,k)=exp(-fac^2/(2*sig_t^2))/(2*pi*sig_t^2);
                sum=sum+w(l,k);
            end
        end
        for k=max(i-floor(rmin),1):min(i+floor(rmin),nex)
            for l=max(j-floor(rmin),1):min(j+floor(rmin),nely)
                w(l,k)=w(l,k)/sum;
                tnew(j,i)=tnew(j,i)+w(l,k)*t(l,k);
            end
        end
        for ely=1:nely
            for elx=1:nex
                if elx==1 || ely==1 || elx==nex || ely==nely
                    tnew(ely,elx)=t(ely,elx);
                end
            end
        end
    end
end
end
function [FCR,df1]=fiber_constraint(nex,nely,t,rmin)
F1=0.;df1=zeros(nely,nex);f1=0;
for i=1:nex
    for j=1:nely
        for k=max(i-floor(rmin),1):min(i+floor(rmin),nex)
            for l=max(j-floor(rmin),1):min(j+floor(rmin),nely)
                F1=F1+1;
                f1=f1+0.99*cos(t(j,i)-t(l,k));
                df1(j,i)=df1(j,i)+0.99*sin(t(j,i)-t(l,k));
            end
        end
        F1=F1-1;f1=f1-1;
    end
end
FCR=f1/F1;
end
function [t,change,xold1,xold2,low,upp,loop,move]=mma...
    (nex,nely,change,loop,df,t,fcr,FCR,dc_t,c,move,...
    angle,m,n,xold1,xold2,low,upp)
loop(2)=loop(2)+1;

```

```

if fcr-FCR>0
    dfdx=df;
else
    dfdx=zeros(nely,nelx);
end
dfdx=dfdx(:);
xval=t(:);
fval=max(0,10000*fcr-FCR*10000);
df0dx=dc_t(:);
f0val=c;
move=0.95*move;
xmax=min(angle+pi/2,xval+move);
xmin=max(angle-pi/2,xval-move);
a0=1;a1=0;c1=1000;d1=0;
[xmma,~,~,~,~,~,~,low,upp] = mmasub...
    (m,n,loop,xval,xmin,xmax,xold1,xold2, ...
    f0val,df0dx,0,fval,dfdx,0,low,upp,a0,a1,c1,d1);
tnew=reshape(xmma,nely,nelx);
xold2=xold1;
xold1=t(:);
change(2)=max(abs(t(:)-tnew(:)));
t=tnew;
end

```

References

- Bendsøe, M.P.; Sigmund, O. *Topology Optimization—Theory, Methods and Applications*; Springer Science & Business Media: Berlin/Heidelberg, Germany, 2003.
- Christensen, R.M. *Mechanics of Composite Materials*; Courier Corporation: Boca Raton, FL, USA, 2012.
- Stegmann, J.; Lund, E. Discrete material optimization of general composite shell structures. *Int. J. Numer. Methods Eng.* **2005**, *62*, 2009–2027. [[CrossRef](#)]
- Hvejsel, C.F.; Lund, E. Material interpolation schemes for unified topology and multi-material optimization. *Struct. Multidiscip. Optim.* **2011**, *43*, 811–825. [[CrossRef](#)]
- Wu, C.; Gao, Y.; Fang, J.; Lund, E.; Li, Q. Discrete topology optimization of ply orientation for a carbon fiber reinforced plastic (CFRP) laminate vehicle door. *Mater. Des.* **2017**, *128*, 9–19. [[CrossRef](#)]
- Mastroddi, F.; Tozzi, M.; Capannolo, V. On the Use of Geometry Design Variables in the MDO Analysis of Wing Structures with Aeroelastic Constraints on Stability and Response. *Aerosp. Sci. Technol.* **2011**, *15*, 196–206. [[CrossRef](#)]
- Ye, H.; Dong, Y.; Yang, J.; Wang, W.; Cheng, M. Concurrent optimization method of principal stress orientation interpolated continuous fiber angle (PSO-CFAO) and structural topology. *Compos. Struct.* **2023**, *325*, 117572. [[CrossRef](#)]
- Jiang, D.; Hoglund, R.; Smith, D. Continuous fiber angle topology optimization for polymer composite deposition additive manufacturing applications. *Fibers* **2019**, *7*, 14. [[CrossRef](#)]
- Smith, D.E.; Hoglund, R. Continuous fiber angle topology optimization for polymer fused filament fabrication. In Proceedings of the 2016 International Solid Freeform Fabrication Symposium, Austin, TX, USA, 8–10 August 2016.
- Almeida, J.H.S., Jr.; Christoff, B.G.; Tita, V.; St-Pierre, L. A concurrent fibre orientation and topology optimisation framework for 3D-printed fibre-reinforced composites. *Compos. Sci. Technol.* **2023**, *232*, 109872. [[CrossRef](#)]
- Gandhi, Y.; Minak, G. A review on topology optimization strategies for additively manufactured continuous fiber-reinforced composite structures. *Appl. Sci.* **2022**, *12*, 11211. [[CrossRef](#)]
- Chen, Y.; Ye, L. Topological design for 3D-printing of carbon fiber reinforced composite structural parts. *Compos. Sci. Technol.* **2021**, *204*, 108644. [[CrossRef](#)]
- Bendsøe, M.P. Optimal shape design as a material distribution problem. *Struct. Optim.* **1989**, *1*, 193–202. [[CrossRef](#)]
- Duvaut, G.; Terrel, G.; Léné, F.; Verijenko, V.E. Optimization of fiber reinforced composites. *Compos. Struct.* **2000**, *48*, 83–89. [[CrossRef](#)]
- Setoodeh, S.; Gürdal, Z.; Watson, L.T. Design of variable-stiffness composite layers using cellular automata. *Comput. Methods Appl. Mech. Eng.* **2006**, *195*, 836–851. [[CrossRef](#)]
- Panesar, A.S.; Weaver, P.M. Optimization of blended bistable laminates for a morphing flap. *Compos. Struct.* **2012**, *94*, 3092–3105. [[CrossRef](#)]
- Desai, A.; Mogra, M.; Sridhara, S.; Kumar, K.; Sesha, G.; Ananthasuresh, G.K. Topological-derivative-based design of stiff fiber-reinforced structures with optimally oriented continuous fibers. *Struct. Multidiscip. Optim.* **2021**, *63*, 703–720. [[CrossRef](#)]
- Guo, S.; Cheng, W.; Cui, D. Aeroelastic Tailoring of Composite Wing Structures by Laminate Layup Optimization. *AIAA J.* **2006**, *44*, 3146–3149. [[CrossRef](#)]

19. de Souza, C.E.; de Leon, D.M. A two-level strategy for aeroelastic optimization of a 3D wing with constant and variable stiffness skins. *Eng. Optim.* **2023**, *55*, 1–20. [[CrossRef](#)]
20. Peeters, D.M.; Lozano, G.G.; Abdalla, M.M. Effect of steering limit constraints on the performance of variable stiffness laminates. *Comput. Struct.* **2018**, *196*, 94–111. [[CrossRef](#)]
21. Jantos, D.R.; Hackl, K.; Junker, P. Topology optimization with anisotropic materials, including a filter to smooth fiber pathways. *Struct. Multidiscip. Optim.* **2020**, *61*, 2135–2154. [[CrossRef](#)]
22. Huang, Y.; Tian, X.; Zheng, Z.; Li, D.; Malakhov, A.V.; Polilov, A.N. Multiscale concurrent design and 3D printing of continuous fiber reinforced thermoplastic composites with optimized fiber trajectory and topological structure. *Compos. Struct.* **2022**, *285*, 115241. [[CrossRef](#)]
23. Schmidt, M.P.; Couret, L.; Gout, C.; Pedersen, C.B. Structural topology optimization with smoothly varying fiber orientations. *Struct. Multidiscip. Optim.* **2020**, *62*, 3105–3126. [[CrossRef](#)]
24. Papapetrou, V.S.; Patel, C.; Tamijani, A.Y. Stiffness-based optimization framework for the topology and fiber paths of continuous fiber composites. *Compos. Part B Eng.* **2020**, *183*, 107681. [[CrossRef](#)]
25. Boddeti, N.; Tang, Y.; Maute, K.; Rosen, D.W.; Dunn, M.L. Optimal design and manufacture of variable stiffness laminated continuous fiber reinforced composites. *Sci. Rep.* **2020**, *10*, 16507. [[CrossRef](#)] [[PubMed](#)]
26. Chandrasekhar, A.; Mirzendehtel, A.; Behandish, M.; Suresh, K. FRC-TOuNN: Topology optimization of continuous fiber reinforced composites using neural network. *Comput.-Aided Des.* **2023**, *156*, 103449. [[CrossRef](#)]

Disclaimer/Publisher’s Note: The statements, opinions and data contained in all publications are solely those of the individual author(s) and contributor(s) and not of MDPI and/or the editor(s). MDPI and/or the editor(s) disclaim responsibility for any injury to people or property resulting from any ideas, methods, instructions or products referred to in the content.